Enhanced coastal shoreline modelling using an Ensemble Kalman Filter to include non-stationarity in future wave climates

Raimundo Ibaceta[1], Kristen D. Splinter[1], Mitchell D. Harley[1] and Ian L. Turner[1]

[1] Water Research Laboratory, School of Civil and Environmental Engineering UNSW Sydney, NSW 2052, Australia.

Corresponding author: Raimundo Ibaceta (r.ibacetavega@unsw.edu.au)

Key Points

- A data-assimilation Dual State-Parameter Ensemble Kalman Filter (EnKF) methodology is integrated within an established shoreline model
- Non-stationary model parameters are obtained, with the accuracy and sampling frequency of shoreline data critical to overall EnKF skill
- Time-varying model parametrizations are physically linked to non-stationary wave forcing, resulting in more accurate shoreline predictions

Abstract

A novel approach to improve seasonal to interannual sandy shoreline predictions is presented, whereby model free parameters can vary in time, adjusting to potential non-stationarity in the underlying model forcing. This is achieved by adopting a suitable data assimilation technique (Dual State-Parameter Ensemble Kalman Filter) within the established shoreline evolution model, ShoreFor. The method is first tested and evaluated using synthetic scenarios, specifically designed to emulate a broad range of natural sandy shoreline behavior. This approach is then applied to a real-world shoreline dataset, revealing that time-varying model free parameters are linked through physical processes to changing characteristics of the wave forcing. Greater accuracy of shoreline predictions is achieved, compared to existing stationary modelling approaches. It is anticipated that the wider application of this method can improve our understanding and prediction of future beach erosion patterns and trends in a changing wave climate.

Plain Language Summary

Understanding and predicting future changes along sandy coastlines worldwide is highly relevant for coastal management in the context of climate change. In the future, the changing occurrence of storms – and over longer timescales, rising sea levels - are expected to result in new patterns of shoreline erosion. It is very common for shoreline change models to use past records of measured shorelines and waves to match mathematical equations to these existing observations. However, the validity of these types of shoreline models to predict the future is questionable, when waves and storm patterns around the world in coming decades are now expected to be different to those observed in the past. A new methodology is presented to address this issue by exploring how a mathematical shoreline model can self-adjust to wave climates that vary through time. The proposed methodology is shown to be successful at improving shoreline predictions.

1 Introduction

Coastal managers have an increasing need for reliable tools that predict the response of sandy coastlines worldwide to the impacts of extreme storm events, shifting regional wave climates and rising sea levels. Semi-empirical shoreline models are proving to be increasingly successful at predicting shoreline variability and evolution at seasonal to multiyear timescales (e.g., Splinter et al., 2014; Yates et al., 2009). However, the complex spatio-temporal interactions of the different processes driving shoreline change make multi-decadal predictions challenging (Montaño et al., 2020), limiting our confidence on shoreline predictions at timescales extending to decades and beyond (Ranasinghe, 2020).

The present generation of shoreline models typically rely on a single period of measured wave forcing and observed shoreline measurements to establish the 'optimum' set of model free parameters (e.g., Long & Plant, 2012). It is then assumed that differences between predicted and measured shorelines can arise from further unresolved morphological processes, inaccuracy in shoreline measurements and/or uncertainty in wave measurements (Montaño et al., 2020). But crucially, by this approach it is implicitly assumed that all model free parameters are stationary, even though the calibrated model may then be used to explore past and future shoreline patterns and trends (e.g., Antolínez et al., 2019; Vitousek et al., 2017). This use of a time-invariant approach to model free parameter estimation necessarily precludes the consideration of potential biases introduced by the particular time period and/or duration of the selected wave and shoreline dataset (D'Anna et al., 2020; Splinter et al., 2013) that is used to perform the calibration. Recent works (D'Anna et al., 2020; Montaño et al., 2020) confirm that shoreline hindcasting and forecasting is highly dependent on the selected calibration period. In the context of a changing climate - and as a result, anticipated temporal variability in the key wave and water-level drivers of shoreline evolution (Wong et al., 2014) - this assumption of model free parameter stationarity must be further examined.

Other fields of geophysical research provide useful guidance on the implementation and physical interpretation of non-stationary model parametrization. For example, Gove & Hollinger (2006) applied a dual state-parameter Unscented Kalman Filter to explore the time evolution of model parameters in problems of surface-atmosphere exchange, in which the observed changes were

linked to seasonal atmospheric-driven variability. More recently, hydrological applications have examined adjustments in rainfall-runoff parametrizations to improve model prediction capabilities resulting from dynamic catchments (e.g., Grigg & Hughes, 2018; Pathiraja et al., 2016a) and climate variability (e.g., Stephens et al., 2019; Xiong et al., 2019). Applied to shoreline modelling, Splinter et al. (2017) used a simplified methodology of split-calibration spanning two consecutive 4-year time periods at the Gold Coast, Australia. By this exploratory approach, a substantial difference in one of the key model free parameters (frequency response) was observed. This was found to be consistent with the finding of a significant difference in the occurrence and distribution of storm wave events between the two consecutive calibration periods. As is illustrated in Figure 1, it was observed that the shoreline response shifted from a distinctly seasonally-dominated mode (annual cycle) to a more storm-dominated (~monthly) mode of behavior, highlighting the challenge of assuming wave climate stationarity when applied to multi-year shoreline prediction and forecasting.

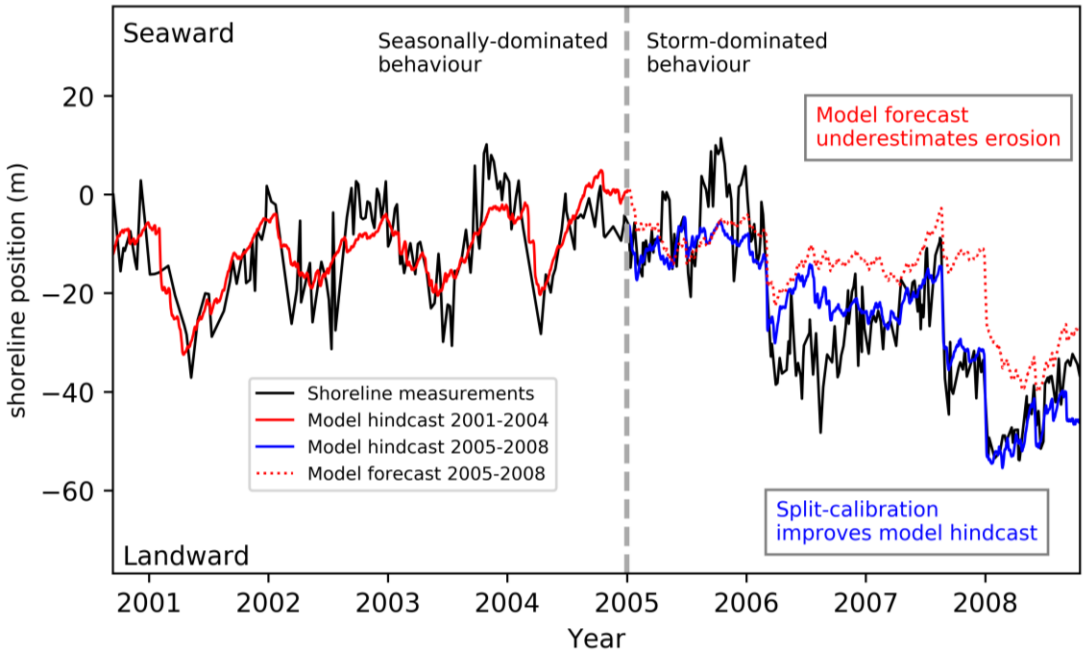

Figure 1. Shoreline observations and modelling for an 8-year period at the Gold Coast, Australia, adapted from Splinter et al., (2017). With the model first calibrated to the 4-year period up to the start of 2005 (red solid line) then used to forecast the shoreline during 2005–2008 (red dotted line), the model was found to significantly underestimate the observed shoreline erosion (black solid line) from 2005 onwards. Subsequent analysis of the Gold Coast wave climate during 2001-2004 found that it was distinctly seasonal during this period, in contrast to the following 4-years 2005-2008 when the wave climate at the Gold Coast was dominated by the

occurrence of individual storm events. To improve model predictions spanning 2005-2008, a second calibration was reported (blue solid line) specific to this time period. Only by applying this 'split calibration' approach could reasonable hindcasts of shoreline behaviour spanning the full 8 years be achieved.

In a recent review of climate change-driven coastal erosion modelling, Toimil et al. (2020) concluded that uncertainty across all constituents of the modelling framework, including model parameters, should be considered. To achieve this objective, data assimilation techniques offer the potential to continuously adjust model parameters as additional state (i.e., shoreline) observations become available (Evensen, 2010). In the new work presented here, a novel methodology to enhance sandy shoreline modelling is developed, in which a suitable data assimilation technique is integrated within an established shoreline evolution model. A Dual State-Parameter Ensemble Kalman Filter (EnKF) (Pathiraja et al., 2016b) is adapted for this purpose, and implemented within the generalized version of the cross-shore ShoreFor model (Splinter et al., 2014). The approach is first tested using synthetic wave climate scenarios, specifically designed to emulate a range of distinct and naturally occurring sandy shoreline behavior. The technique is then applied to a real-world observational dataset, where it is determined that the time-variation in model free parameters can be linked through physical processes to the changing characteristics of the wave forcing at this long-term study site.

2 Methods

2.1 Shoreline Model

ShoreFor (Davidson et al., 2013) is a semi-empirical model based on the behavioral concept that shorelines continuously evolve towards a time-varying equilibrium position. In the generalized form of this model (Splinter et al., 2014; hereafter SPLI14), the cross-shore rate of shoreline change (*dx/dt*) is given by:

$$\frac{dx}{dt} = c^a F^a + c^e F^e + b \qquad (1)$$

whereby the forcing term $F^{a,e} = P^{0.5}\,\Delta\Omega_{a,e}/\sigma_{\Delta\Omega}$ accounts for the wave power (P) and the disequilibrium dimensionless fall velocity ($\Delta\Omega$), which in turn dictates the potential direction either offshore ($\Delta\Omega_e < 0$) or onshore ($\Delta\Omega_a > 0$) of cross-shore sediment transport. Within this forcing term the disequilibrium component $\Delta\Omega = (\Omega_{eq} - \Omega)$ and its associated standard deviation $\sigma_{\Delta\Omega}$ are computed from the dimensionless fall velocity Ω at the break point (i.e., the

seaward edge of the surf zone) and a time-varying equilibrium expression (after Wright et al., 1985) given by:

$$\Omega_{eq} = \left[\sum_{i=1}^{2\phi} 10^{-i/\phi}\right]^{-1} \sum_{i=1}^{2\phi} \Omega_i 10^{-i/\phi} \qquad (2)$$

Note that the additional term b in (1) simply accounts for any unresolved processes. Importantly, the model in Equation 1 includes three wave-driven sediment transport-related parameters c^a, c^e and ϕ that require calibration. The magnitude rate parameters c^a and c^e (in $m^{1.5}s^{-1}W^{-0.5}$) are proxies for the accretion/erosion sediment transport efficiency, and the frequency rate parameter ϕ (in days) represents a response time. Based on extensive testing of the ShoreFor model at a diverse range of seasonal and storm-dominated sandy coastlines in Australia, Europe and the USA, SPLI14 proposed generalized parametrizations for these rate parameters based on the mean interannual ($\geq \sim$5 years) $\bar{\Omega}$, consistent with well-established relationships (e.g., Wright and Short, 1984) between modal beach states and cross-shore processes. Conceptually, mild-slope beaches experience slower rates of shoreline changes (i.e. $\phi > 100$ days) and decreased sediment exchange efficiency (lower c^a and c^e values) between the surf zone and beach face. Conversely, the breaker line tends to be closer to the beach face at steeper beaches, enhancing efficient (larger c^a and c^e magnitudes) and rapid (i.e. $\phi < 100$ days) sediment exchange. Within this framework, Davidson et al., (2013) found that $\phi \cong 100$ days usefully defines the approximate transition between storm-dominated and more seasonal shoreline response. The reader is referred to Davidson et al., (2013) and SPLI14 for a complete description of the model.

2.2 Synthetic scenarios with the ShoreFor model

Ten shoreline timeseries each spanning 20-years at 3-hourly sampling intervals were generated using ShoreFor, forced by a set of synthetic wave records based on real observations and specifically designed to characterize seasonal, storm and mixed seasonal-storm wave climates. As is summarized in Figure 2a, four shape functions were defined to represent differing modes of wave climate variability and long-term trends: simple time-invariant (Shape 1), a linear negative trend (Shape 2), a sinusoidal function with a representative period of 10 years (Shape 3) and a step-wise function (Shape 4). To generate the 10 synthetic scenarios, these four parameter shapes were then mixed together with increasing degree of complexity. A full description of this process

is detailed in the accompanying Supporting Information. As the focus here is on the non-stationarity of wave-driven parameters, for all ten scenarios $b = 0$ (see Equation 1).

The resulting shoreline timeseries are then subsampled at time intervals (dt) of 1, 7, 15 and 30 days, representative of a range of typical sampling frequencies used for ongoing shoreline monitoring programs worldwide (e.g., Holman & Stanley, 2007; Turner et al., 2016) and random noise added ($\sim N(0, R^2)$, R=[1,1,12] m) to characterize the accuracy of various shoreline measurement methods that are typically used (see Harley et al., 2011). The final result is a total of 480 individual test cases. For a number of these cases it is anticipated (see Figure S1b, Supporting Information) that model parameter variability may be modulated and therefore not necessarily stationary at both multiyear (say, 5-10 years) and longer inter-decadal timescales, responding to climate patterns (e.g. ENSO) as well as longer-term trends in wave climate (e.g., Young & Ribal, 2019). In contrast, shoreline changes below these timescales are anticipated to be well-resolved by the existing SPLI14 stationary approach to model parameter calibration. Figures S2–S4 in the accompanying Supporting Information present the synthetic shoreline and parameter timeseries for each of the 10 scenarios.

2.3 Dual State-Parameter Ensemble Kalman Filter

To explore parameter non-stationarity within the context of an established shoreline model, the Dual State-Parameter EnKF algorithm proposed by Pathiraja et al., (2016b, 2016a) was implemented. The full details of the methodology are summarized in Figure S5 of the accompanying Supporting Information. Briefly, for each algorithm realization the method initializes system states (i.e., shorelines) and model parameters as random variables created from *n* ensemble members of known mean and error characteristics, and propagates these in time as a Monte Carlo application of the well-known Kalman Filter (Evensen, 2010).

At each 3-hourly time-step, the shoreline model first uses inflated (i.e. process noise included) background parameter ensembles to estimate shorelines at the next time-step. This continues until a new shoreline observation is available, which in turn is dependent on the particular sampling frequency (dt). At this point, parameter ensembles are updated based on the shoreline observation ensembles (i.e. mean with error statistics mirroring the measurement accuracy, R in Section 2.2). These updated parameters are then used to provide new shoreline estimates, which

are then used to calculate combined mean-confidence intervals of both the shorelines and model parameters. Pathiraja et al., (2016b) found that the magnitude of parameter ensemble inflation (process noise) was critical to successfully track parameter changes, otherwise updated estimates with lower variance than the previous time-step resulted in nearly time-invariant parametrizations (e.g., Long & Plant, 2012; Vitousek et al., 2017). In the present work, the approach of Xiong et al., (2019) was implemented, in which the magnitude of process noise was sufficiently high to track time-varying parametrizations. Further details are provided in the Supporting Information.

Initial parameter ensembles are generated from truncated normal distributions to ensure that parameters fall within their feasible range (Splinter et al., 2014). Rather than correcting for erroneous initial parameter values, the purpose is to assess the EnKF performance for tracking the potential non-stationarity of some or all model parameters. Therefore, the optimum initial conditions with standard deviation spanning the range of values previously determined by Splinter et al., (2014) were implemented. The exceptions to this approach were for Scenarios 1 and 2, since these cases are fully time-invariant, so instead random initial conditions sampled from a uniform distribution were adopted. An analysis (not shown) for Scenario 10 using ensemble sizes of n = 10, 25, 50, 100, 250 and 500 members showed similar results for all cases where $n \geq 50$ and thus we adopt n = 50 for computational efficiency. Ensemble statistics were computed over 50 realizations of the algorithm, to account for the stochastic nature of the EnKF (Pathiraja et al., 2016b). Thus, a total of 24000 individual model runs were used to explore the EnKF performance to varying wave climate, shoreline measurement frequency and accuracy, and degrees of parameter variability.

a)

Scenario	1 ▲	2 ●	3 ▲	4 ●	5 ▲	6 ●	7 ▲	8 ●	9 ◆	10 ◆
Wave climate	Seasonal	Storm	Seasonal	Storm	Seasonal	Storm	Seasonal	Storm	Mixed	Mixed
Shape 1	$c^{a,e}$, ϕ	$c^{a,e}$, ϕ	c^{e}, ϕ	c^{e}, ϕ	ϕ	ϕ	ϕ	ϕ	$c^{a,e}$	
Shape 2			c^{a}	c^{a}			c^{a}	c^{a}		c^{a}
Shape 3					$c^{a,e}$	$c^{a,e}$	$c^{a,e}$	$c^{a,e}$		$c^{a,e}$
Shape 4									ϕ	ϕ

b)

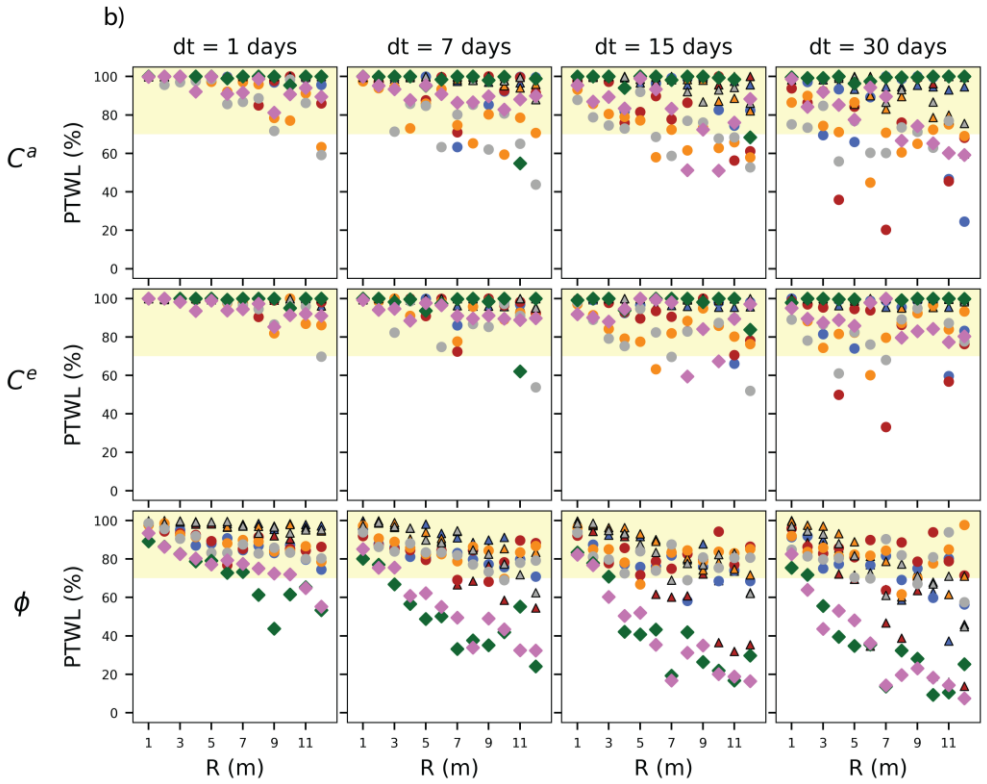

Figure 2. Ten synthetic shoreline scenarios generated with ShoreFor and sampled at a range of frequencies, incorporating increasingly complex combinations of parameter variability and a range of synthetic wave climates. (a) The four shape functions are: time-invariant (Shape 1), a linear negative trend (Shape 2), a sinusoidal function with a representative period of 10 years (Shape 3) and a step-wise function (Shape 4). As is tabulated, these are then applied in an increasingly complex combination of time-varying model parameters and either a seasonal, storm-driven or mixed seasonal-storm wave climate. (b) EnKF skill expressed as the percentage of time within acceptable limits (PTWL), when applied at different sampling frequencies dt = 1, 7, 15 & 30 days. These results are summarised for the three ShoreFor wave-driven parameters c^a, c^e, ϕ (top to bottom) as a function of shoreline measurement accuracy R (horizontal axes). Note that higher PTWL values indicate superior algorithm performance. Triangles (circles) correspond to cases generated by the seasonal (storm) dominated wave climate scenarios 1 - 8. Diamonds correspond to the mixed seasonal-storm wave climates in scenarios 9 and 10.

3 Results

3.1 Synthetic Cases

The performance of the EnKF is summarized in Figure 2b for the three wave-driven parameters c^a, c^e, ϕ (from top to bottom), different shoreline time-sampling dt = 1, 7, 15 and 30 days (from left to right) and shoreline measurement accuracy R = 1:1:12 m (horizontal axes). The percentage of time the ensemble mean is within acceptable limits (denoted PTWL, after Pathiraja et al., 2016b) is used as the performance metric, such that PTWL values closer to 100% indicate higher skill. Acceptable limits are defined for time t as $\theta_t^* + \rho d_p$, where θ_t^* is the true synthetic parameter magnitude, d_p is the feasible range of parameters magnitude (SPLI14) and ρ is the 10% fraction. A benchmark of PTWL $\geq$ 70% is selected here to define cases where the EnKF methodology could be reasonably anticipated to succeed when applied to real-world datasets. Accordingly, 87% of the cases fulfil this condition. In general, results indicate that the EnKF performance is highly dependent on the quality of the observational data, whereby more frequently sampled and less-noisy measured shorelines result in higher PTWL for the majority of scenarios.

To explore this general conclusion in further detail, representative results for the highest quality shoreline data (dt = 1 day, R = 1 m) are shown in Figure 3a-d for increasingly complex Scenarios 4, 5, 9 and 10, respectively. From top to bottom, panels show the EnKF estimations (shown in black) of shoreline timeseries as well as the parameters c^a, c^e and ϕ, compared to their true synthetic values (red dashed lines). Time-invariant (Shape 1), negative trend (Shape 2), sinusoidal (Shape 3) and step-wise parameter functions (Shape 4) are well estimated by the EnKF for the full range of idealized seasonal, storm and mixed wave climates.

Examples of parameter estimation sensitivity to varying shoreline measurement accuracy (R = 1, 4, 8 and 12 m, dt = 7 days) and frequency (dt = 1, 7, 15 and 30 days, R = 4 m) are shown in Figure 3e-f for the complex Scenario 10. As anticipated, EnKF performance decreases for higher levels of R (e.g. ϕ, Figure 3e). With decreasing observational quality data, parameter convergence is slower as the EnKF algorithm weights the model equations more than the observations (e.g., Long & Plant, 2012; see also S2 in Supporting Information).

The effect of decreasing the frequency of shoreline observations (i.e. increasing dt) is also apparent, resulting in less accurate and time-lagged parameter estimations (e.g. ϕ, Figure 3f). However, Figure 2b demonstrates that results are more sensitive to observation accuracy (R) rather than observation frequency (dt), with this being most pronounced for variations in ϕ (lower panels). The time-lag between true and estimated parameters is assessed through the convergence time of initially random sampled parameters at Scenarios 1 and 2 (fully time-invariant). For all values of R and dt, 73% of the time-invariant cases (Figure 2, blue circles and triangles) converge within 2 years (i.e. PTWL > 90%). Notably, convergence and the ability to capture time variability are inversely dependent on the level of process noise. For example, adopting a lower process-noise (e.g., Long & Plant, 2012; Vitousek et al., 2017) results in 92% of the time-invariant cases converging, however, this low level of noise severely limits the EnKF performance on non-stationary parametrizations (Pathiraja et al., 2016b). It is therefore concluded that the approach presented here is well suited to identifying and interpreting model parameter non-stationarity using the established ShoreFor model at timescales down to interannual. Notably, this convergence time is similar to Long and Plant (2012) who used an Extended Kalman Filter applied to synthetic monthly-sampled shorelines of R = 0.5 m accuracy. The new and more extensive analyses presented here provides the encouraging result that, for shoreline measurement accuracy that can be more realistically obtained in the field (i.e., R up to 12 m) the EnKF performs well. Results for Scenarios 9 and 10 (Figure 2b) also indicate that ϕ estimations are in general less accurate than those for c^a and c^e. This is because the time-varying equilibrium expression given by Equation 2 is relatively insensitive for values of ϕ > 100 days, resulting in the potential for parameter equifinality and lower parameter estimation quality (e.g., Figure 3f, at around year 11).

The effect of differing wave climate characteristics can be also explored for varying levels of shoreline measurement accuracy. Selecting a representative sampling interval of dt = 7 days and comparing similar parameter combinations forced by the seasonally-dominated Scenario 5 (Figure 3g) versus the storm-dominated Scenario 6 (Figure 3h), results indicate an overall higher skill level for the seasonal cases, up to and including the least-accurate shoreline data considered here (R = 12 m). This observation is attributed to the more frequent and rapidly varying

characteristics of an episodic storm wave climate, compared to the more slowly evolving characteristics of a seasonal wave climate.

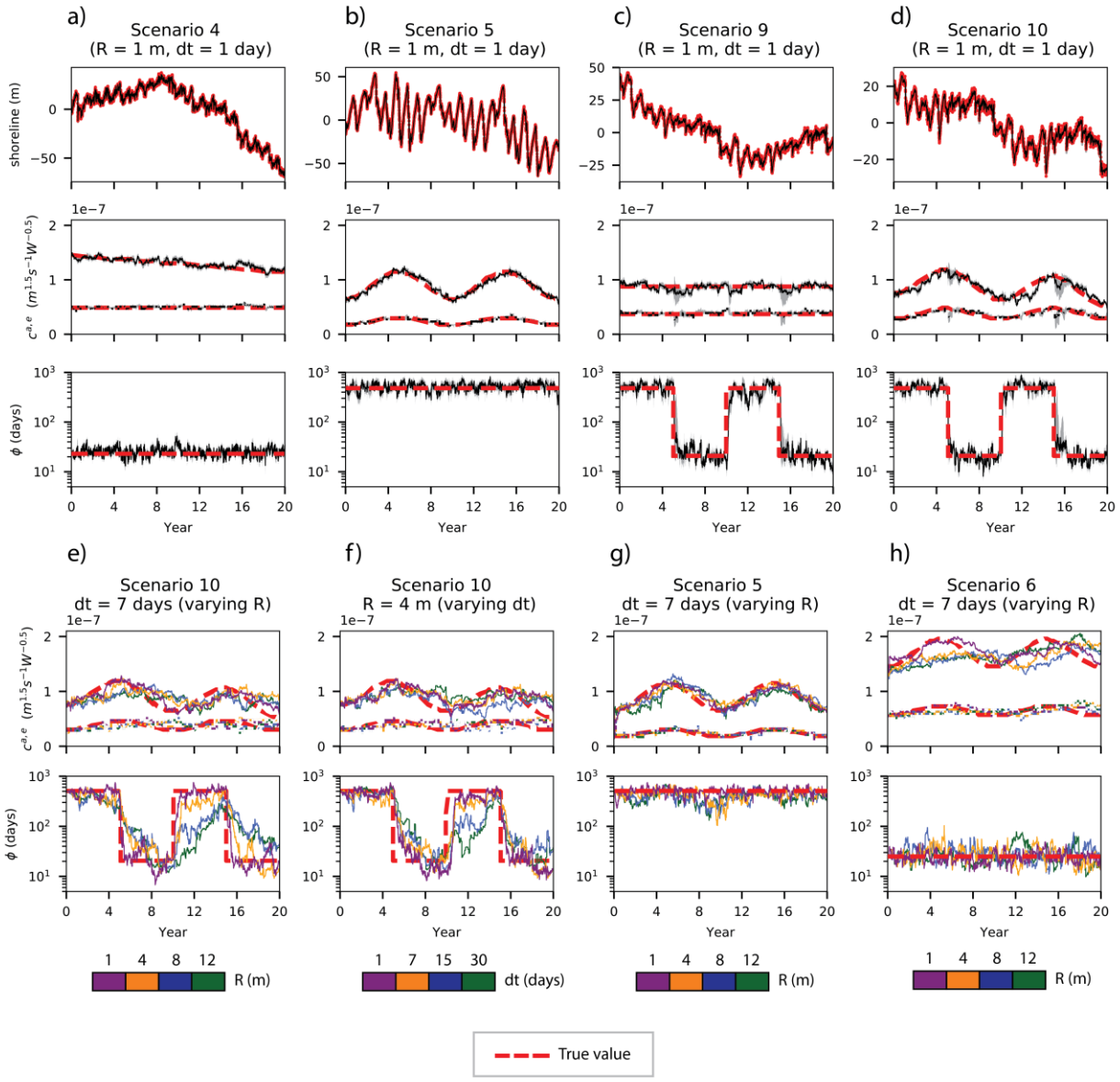

Figure 3. Representative results of the EnKF algorithm. Examples for the highest quality shoreline data (R = 1 m and dt = 1 day) are shown in (a)-(b)-(c)-(d) (from top to bottom, shorelines, c^a, c^e and ϕ, note that $c^a > c^e$) for Scenarios 4, 5, 9 and 10, respectively. Black lines are the EnKF estimates, red dashed lines are the true synthetic values and grey bands indicate the central 95% ensemble. Algorithm sensitivity to dt and R is shown (Scenario 10) for (e) varying R (at dt = 7 days) and (f) varying dt (at R = 4 m). Depictive examples for algorithm sensitivity to wave climate characteristics are shown for Scenarios 5 and 6 which are generated from (g) seasonal and (h) storm-dominated wave climate, respectively. Note that parameter confidence bands in (e), (f), (g) and (h) were not included to better facilitate visualization.

3.2 Application to a real-world shoreline dataset

The EnKF technique is now applied to a dataset of measured shorelines and waves at the Gold Coast in southeast Australia spanning the 8-year period 2001-2008. This same shoreline dataset was previously described in Splinter et al., (2017; hereafter SPLI17) and is also shown in Figure 1, being notable because of the observation that shoreline variability switched from a distinctly seasonally-dominated mode to an episodic storm-dominated mode mid-way through the 8-year measurement period. Briefly, to obtain this dataset shorelines were obtained on a weekly basis (dt = 7 days) from ARGUS video imagery (Holman & Stanley, 2007) with a cross-shore accuracy of R ~ 5 m (Turner & Anderson, 2007). Wave buoy and shoreline observations are assimilated into the ShoreFor model equations. As this is a real-world dataset, in contrast to the synthetic cases (Section 3.1) the last term in Equation 1 is no longer fixed as $b = 0$, to account for the possibility of secondary processes. The focus of the results presented here, however, remains on the primary wave-driven cross-shore model parameters. To apply the new EnKF methodology, initial model parameter estimates were obtained via the generalized parametrizations provided in SPLI14 applied to the first 4-years of the wave record, along with an initial seed value of $b = 0$. To explore and compare the new non-stationary EnKF results to previous time-invariant approaches, three additional ShoreFor model realizations are presented: 1) a single calibration spanning the full 8-year dataset; 2) split-sample calibration of the two consecutive time-periods T1 (2001-2004) and T2 (2005-2008) as reported in SPLI17 (see Figure 1); and 3) use of the stationary model free parameters derived for T1 to forecast the shoreline variability in T2.

A summary of these results is presented in Figure 4. From top to bottom, Figure 4a shows the shoreline predictions for the four different ShoreFor model realizations, along with in Figure 4b and 4c the corresponding values of non-stationary/stationary model free parameters c^a (continuous lines), c^e (dashed lines) and ϕ. As was previously observed in SPLI17, Figure 4 demonstrates that shoreline and parameter estimation is sensitive to the selected calibration period, bringing into question the validity of the assumption of stationarity. Encouragingly, comparison of the new non-stationary EnKF approach (Figure 4a, black line) that now enables the model free parameters to continuously evolve in time, can be seen to result in enhanced model skill (EnKF, ρ=0.95, NMSE=0.10, RMSE=5.0 m) when compared to the stationary

calibration (Figure 4a, magenta line) based on the 8-year dataset (8-year, ρ =0.82, NMSE=0.33, RMSE=8.8 m).

SPLI17 relied on subjective visual observation to distinguish the two time periods of T1 and T2 to undertake the reported split calibration. A key advantage of the new EnKF approach is that it is able to continuously vary model parameters to best fit the shoreline observations. In particular, after an initial period (2001-2003) of increasing magnitudes in c^a and c^e, the multi-year variability of both parameters from 2004 onwards (Figure 4b, black line) converges more closely to the magnitudes obtained in the T2 stationary calibration. Both c^a and c^e also show shorter-term variability (~seasonal) which remains unexplained and outside the scope of the present work. These changes suggest a relationship of this variability in c^a and c^e and an underlying change in the forcing wave climate that requires further investigation (See Discussion). As was previously determined for the synthetic cases (Section 3.1), ϕ is the most challenging parameter to estimate primarily because the model is relatively insensitive for $\phi > 100$ days (see Section 2.1). In the Gold Coast real-world application presented here (Figure 4c), during the time period T1 the time-evolving ϕ remains large ($\phi \cong 1000$ days) and relatively constant, corresponding to a more seasonally dominated mode of shoreline behavior. In contrast, during the following T2 period this parameter can be seen to deviate and vary substantially from this value, oscillating towards lower magnitudes ($\phi \cong 100$ days) that are more indicative of a period of storm-dominated shoreline behavior.

The final model realization depicted in Figure 4 shows the effect of transferring stationary model free parameters calibrated from the initial time period T1 into the following T2, analogous to the forecasting of future shoreline behavior (e.g., Davidson et al., 2013). Unlike the EnKF continuous parameter adjustment, the time-invariant approach indicates that the T2 shoreline forecast (Figure 4a, red dotted line) continues to track the general multi-year variability observed during T1, but underestimates shorter-term erosive periods that are encountered during T2 (e.g. 2008). As anticipated, this result highlights the inherent weakness in the assumption of parameter stationarity when semi-empirical shoreline models are applied to out-of-calibration shoreline prediction.

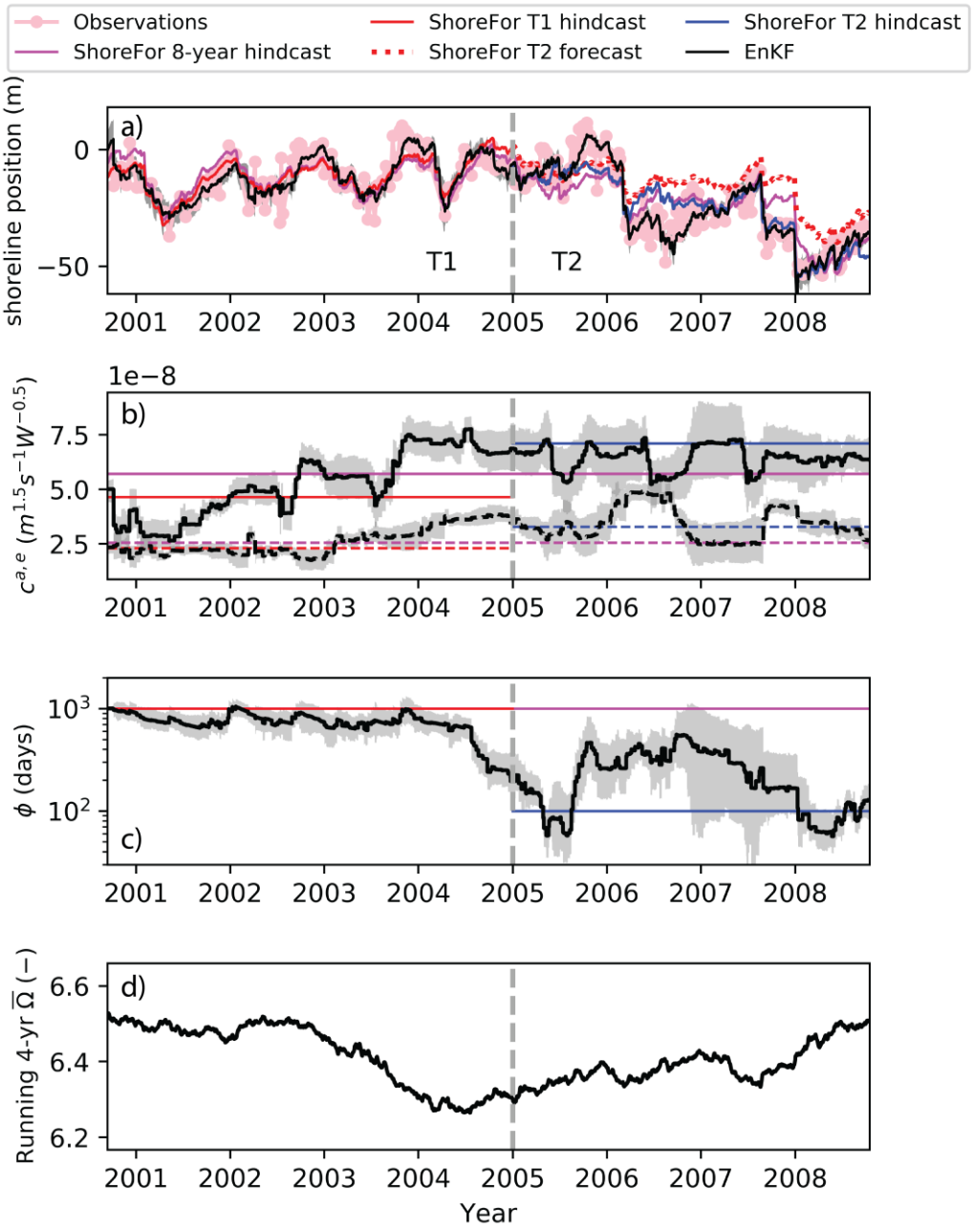

Figure 4. EnKF application to a real observational shoreline dataset at the Gold Coast, Australia, and compared to 3 different time-invariant ShoreFor realizations: 1) overall 8-year period (magenta lines), 2) split-sample calibration (after SPLI17) of two consecutive time-periods T1 (2001-2004, red lines) and T2 (2005-2008, blue lines), and 3) T2 model forecast obtained from T1 model calibration (red dotted lines in panel a). From top to bottom a) Shoreline observations (pink dots), shoreline EnKF estimates (black line), T1 model hindcast (red continuous line), T2 model hindcast (blue line), complete 8-year hindcast period (magenta line) and T2 forecast obtained from T1 model calibration (red dotted line). b) c^a (continuous lines) and c^e (dashed lines) with line colours as described for panel (a). Note that horizontal lines represent time-invariant approaches. Similarly, panel (c) shows the frequency rate parameter (ϕ) estimated with

the EnKF and from time-invariant approaches. Grey bands indicate the central 95% ensembles. (d) Running mean (4-year) dimensionless fall velocity at the wave breaking position.

4 Discussion and Conclusions

Analysis of 480 test cases, comprising ten synthetic shoreline timeseries derived from an increasingly complex mix of four distinct parameter functions, three wave climate characteristics and differing levels of observation accuracy and time-sampling (Section 2.2), confirms that the EnKF technique is suitable for tracking non-stationary parametrizations (PTWL $\geq$ 70%) to predict the cross-shore movement of shorelines at multi-year timescales (Section 3.1). Exceptions to this general conclusion include cases where the observation shoreline data is either too noisy (R > ~6 m) or measured too infrequently (dt > ~15 days), with measurement accuracy and frequency become decreasingly important for beaches exposed to more seasonal compared to storm-dominated wave climates. In addition to the EnKF methodology providing a new enhancement over previous stationary calibration methods by enabling model parameters to evolve in response to non-stationary wave climate forcing, it also facilitates the use of ensemble-based approaches to incorporate uncertainty in both the estimated shorelines and model parameters. This overall improvement to the ability to predict shoreline behavior is illustrated by the real-world application at the Gold Coast presented in Figure 4, where the use of time-varying c^a, c^e and ϕ parameters and their uncertainty result in higher accuracy shoreline predictions spanning the total 8-year observation period.

It is of interest to now briefly consider how the EnKF technique can be extended to explore the underlying physical processes that may be occurring at a coastal site. For example, the Gold Coast application in Section 3.2 reveals time periods commencing in mid-2004 when the magnitude of ϕ shifted from essentially constant to an overall decrease in magnitude and increase in variability (Figure 4c), corresponding to the previously identified switch in the wave climate and resulting shoreline behavior from seasonal to storm-dominated (SPLI17). In addition, the EnKF captures the multiyear variability in c^a and c^e initially indicating an increasing trend (2001-2003), and then roughly constant with some seasonal variability (2004-onwards).

The previous stationary approach detailed in SPLI14 dictates that the accretionary rate term c^a is a function of the mean dimensionless fall velocity ($\bar{\Omega}$) at a site, and then assumes that the erosive rate term c^e is simply proportional to c^a. According to SPLI14 parametrizations, magnitude increases in c^a would necessarily implicate negative trends in the multi-year $\bar{\Omega}$. This relationship between c^a and $\bar{\Omega}$, as well as the assumed proportionality of c^a and c^e appears to be captured by the EnKF during the initial 2001-2003 period. However, the new EnKF results presented here that allow for independent calibration of c^a and c^e, reveal that these two parameters may not be simply proportional to each other, and will require further fundamental physical-process investigation. Interestingly, in the latter half of the data (2005-2008) these two terms appear to oscillate on seasonal to interannual frequency but in opposite directions (e.g. 2006, Figure 4b). Recalling that c^a and c^e in the ShoreFor model encapsulate cross-shore sediment transport efficiency (Section 2.1), this temporal variability may be linked to nearshore morphology. For example, Ruessink et al., (2009) used video images to observe the decay of an outer bar at this site in early 2006. The resulting loss of a protective outer bar and the formation of a new bar close to the shoreline matches with increased/reduced efficiency in erosive (c^e) and accretive (c^a) processes, respectively.

Synthetic and real-world results presented here emphasize the need for shoreline model structure that can adjust to potential changes in the underlying physical forcing. Results of the new work presented here suggest that the EnKF method is able to capture this variability when applied over long-term datasets subjected to natural variability at interannual scales and beyond, and for which waves are the driver of the observed and/or anticipated shorelines changes. The inclusion of time-varying parametrizations (and their uncertainty) offers the opportunity to ensure consistency between modelled coastal evolution drivers and the underlying physical processes (Toimil et al., 2020), and now warrants the EnKF application as a method to explore parameter changes and predict future beach erosion patterns and trends in the face of inter-decadal shifting waves (Morim et al., 2019) and intensified climate teleconnections patterns (Barnard et al., 2015; Mentaschi et al., 2017).

Future applications of the EnKF are likely to be motivated by the advent of newly available global-scale shoreline detection methods (e.g., Kelly & Gontz, 2019; Vos et al., 2019) and the

increasing public availabiltiy of high resolution long-term shoreline datasets (e.g., Ludka et al., 2019; Turner et al., 2016). It is anticipated that the approach presented here will be useful for exploring cross-shore parameter variability as a first step for training model parameters and relating their variability to natural changes in forcing. Shoreline models will also benefit from a clearer understanding and inclusion of cross-shore model parametrizations, ensemble-based wave forcing (e.g. Davidson et al., 2017) and also from the inclusion of additional processes such as alongshore sediment transport and sea level rise (e.g., Robinet et al., 2018; Vitousek et al., 2017). The EnKF approach presented here offers the potential to provide a robust structure to account for uncertainty across all constituents of the shoreline modeling framework (Toimil et al., 2020), as one contributor to the end-goal of achieving realiable multi-decadal shoreline projections. These improved tools will be useful to coastal managers and stakeholders, by providing combined magnitude-uncertainty predictions that can be applied to future hazard assessment and planning.

Acknowledgments and data availability

Wave data from the Gold Coast was provided by Gold Coast City Council (https://www.data.qld.gov.au/dataset/coastal-data-system-waves-gold-coast). Wave data for the seasonal and storm-dominated scenarios was obtained from the CAWCR dataset (http://hdl.handle.net/102.100.100/137152?index=1). ARGUS images from which shorelines were derived are provided by the Water Research Laboratory, UNSW Australia (http://ci.wrl.unsw.edu.au/current-projects/northern-gold-coast-narrowneck-reef/archived-data/) with funding from Gold Coast City Council. Raimundo Ibaceta is funded by NSW Environmental Trust Environmental Research Program (RD2015/0128), UNSW and CONICYT (now ANID) Becas de Doctorado en el Extranjero – Becas Chile N72180087. We acknowledge Sahani Pathiraja and Lucy Marshall for thier initial discussion and assistance with previous applications of EnKF. We also thank Joseph Long for his ideas and discussions during earlier stages of this work.

References

Antolínez, J. A. A., Méndez, F. J., Anderson, D., Ruggiero, P., & Kaminsky, G. M. (2019). Predicting Climate- Driven Coastlines With a Simple and Efficient Multiscale Model. *Journal of Geophysical Research: Earth Surface*, *124*(6), 1596–1624. https://doi.org/10.1029/2018JF004790

Barnard, P. L., Short, A. D., Harley, M. D., Splinter, K. D., Vitousek, S., Turner, I. L., et al. (2015). Coastal vulnerability across the Pacific dominated by El Niño/Southern Oscillation. *Nature Geoscience*, *8*(10), 801–807. https://doi.org/10.1038/ngeo2539

D'Anna, M., Idier, D., Castelle, B., Le Cozannet, G., Rohmer, J., & Robinet, A. (2020). Impact of model free parameters and sea-level rise uncertainties on 20-years shoreline hindcast: the case of Truc Vert beach (SW France). *Earth Surface Processes and Landforms*. https://doi.org/10.1002/esp.4854

Davidson, M A, Splinter, K. D., & Turner, I. L. (2013). A simple equilibrium model for predicting shoreline change. *Coastal Engineering*, *73*, 191–202. https://doi.org/10.1016/j.coastaleng.2012.11.002

Davidson, Mark A, Turner, I. L., Splinter, K. D., & Harley, M. D. (2017). Annual prediction of shoreline erosion and subsequent recovery. *Coastal Engineering*, *130*, 14–25. https://doi.org/10.1016/j.coastaleng.2017.09.008

Evensen, G. (2010). *Data assimilation: The ensemble kalman filter*. *Data Assimilation: The Ensemble Kalman Filter*. https://doi.org/10.1007/978-3-540-38301-7

Gove, J. H., & Hollinger, D. Y. (2006). Application of a dual unscented Kalman filter for simultaneous state and parameter estimation in problems of surface-atmosphere exchange. *Journal of Geophysical Research Atmospheres*, *111*(8), 1–21. https://doi.org/10.1029/2005JD006021

Grigg, A. H., & Hughes, J. D. (2018). Nonstationarity driven by multidecadal change in catchment groundwater storage: A test of modifications to a common rainfall–run-off model. *Hydrological Processes*, *32*(24), 3675–3688. https://doi.org/10.1002/hyp.13282

Harley, M. D., Turner, I. L., Short, A. D., & Ranasinghe, R. (2011). Assessment and integration of conventional, RTK-GPS and image-derived beach survey methods for daily to decadal coastal monitoring. *Coastal Engineering*, *58*(2), 194–205. https://doi.org/10.1016/j.coastaleng.2010.09.006

Holman, R. A., & Stanley, J. (2007). The history and technical capabilities of Argus. *Coastal Engineering*, *54*(6–7), 477–491. https://doi.org/10.1016/j.coastaleng.2007.01.003

Kelly, J. T., & Gontz, A. M. (2019). Rapid Assessment of Shoreline Changes Induced by Tropical Cyclone Oma Using CubeSat Imagery in Southeast Queensland, Australia. *Journal of Coastal Research*, *36*(1), 72. https://doi.org/10.2112/jcoastres-d-19-00055.1

Long, J. W., & Plant, N. G. (2012). Extended Kalman Filter framework for forecasting shoreline evolution. *Geophysical Research Letters*, *39*(13), n/a–n/a. https://doi.org/10.1029/2012GL052180

Ludka, B. C., Guza, R. T., O'Reilly, W. C., Merrifield, M. A., Flick, R. E., Bak, A. S., et al. (2019). Sixteen years of bathymetry and waves at San Diego beaches. *Scientific Data*, *6*(1), 161. https://doi.org/10.1038/s41597-019-0167-6

503 Mentaschi, L., Vousdoukas, M. I., Dosio, A., Voukouvalas, E., & Feyen, L. (2017). Global
504 changes of extreme coastal wave energy fluxes triggered by intensified teleconnection
505 patterns. *Geophysical Research Letters*, 2416–2426. https://doi.org/10.1002/2016gl072488

506 Montaño, J., Coco, G., Antolínez, J. A. A., Beuzen, T., Bryan, K. R., Cagigal, L., et al. (2020).
507 Blind testing of shoreline evolution models, 1–10. https://doi.org/10.1038/s41598-020-
508 59018-y

509 Morim, J., Hemer, M., Wang, X. L., Cartwright, N., Trenham, C., Semedo, A., et al. (2019).
510 Robustness and uncertainties in global multivariate wind-wave climate projections. *Nature*
511 *Climate Change*, *9*(9), 711–718. https://doi.org/10.1038/s41558-019-0542-5

512 Pathiraja, S., Marshall, L., Sharma, A., & Moradkhani, H. (2016a). Detecting non-stationary
513 hydrologic model parameters in a paired catchment system using data assimilation.
514 *Advances in Water Resources*, *94*, 103–119.
515 https://doi.org/10.1016/j.advwatres.2016.04.021

516 Pathiraja, S., Marshall, L., Sharma, A., & Moradkhani, H. (2016b). Hydrologic modeling in
517 dynamic catchments: A data assimilation approach. *Water Resources Research*, *52*(5),
518 3350–3372. https://doi.org/10.1002/2015WR017192

519 Ranasinghe, R. (2020). On the need for a new generation of coastal change models for the 21 st
520 century. *Scientific Reports*, 1–6. https://doi.org/10.1038/s41598-020-58376-x

521 Robinet, A., Idier, D., Castelle, B., & Marieu, V. (2018). A reduced-complexity shoreline change
522 model combining longshore and cross-shore processes: the LX-Shore model. *Environmental*
523 *Modelling and Software*. https://doi.org/10.1016/j.envsoft.2018.08.010

524 Ruessink, B. G., Pape, L., & Turner, I. L. (2009). Daily to interannual cross-shore sandbar
525 migration: Observations from a multiple sandbar system. *Continental Shelf Research*,
526 *29*(14), 1663–1677. https://doi.org/10.1016/j.csr.2009.05.011

527 Splinter, K. D., Turner, I. L., & Davidson, M. A. (2013). How much data is enough? The
528 importance of morphological sampling interval and duration for calibration of empirical
529 shoreline models. *Coastal Engineering*, *77*, 14–27.
530 https://doi.org/https://doi.org/10.1016/j.coastaleng.2013.02.009

531 Splinter, K. D., Turner, I. L., Davidson, M. A., Barnard, P., Castelle, B., & Oltman-Shay, J.
532 (2014). A generalized equilibrium model for predicting daily to inter-annual shoreline
533 response. *Journal of Geophysical Research: Earth Surface*, *119*, 1936–1958.
534 https://doi.org/10.1002/2014JF003106

535 Splinter, K. D., Turner, I. L., Reinhardt, M., & Ruessink, G. (2017). Rapid adjustment of
536 shoreline behavior to changing seasonality of storms: observations and modelling at an
537 open-coast beach. *Earth Surface Processes and Landforms*, *42*(8), 1186–1194.
538 https://doi.org/10.1002/esp.4088

539 Stephens, C. M., Marshall, L. A., & Johnson, F. M. (2019). Investigating strategies to improve

hydrologic model performance in a changing climate. *Journal of Hydrology*, *579*(September), 124219. https://doi.org/10.1016/j.jhydrol.2019.124219

Toimil, A., Camus, P., Losada, I. J., Cozannet, G. Le, Nicholls, R. J., Idier, D., & Maspataud, A. (2020). Climate change-driven coastal erosion modelling in temperate sandy beaches: Methods and uncertainty treatment. *Earth-Science Reviews*, 103110. https://doi.org/https://doi.org/10.1016/j.earscirev.2020.103110

Turner, I. L., & Anderson, D. J. (2007). Web-based and "real-time" beach management system. *Coastal Engineering*, *54*(6–7), 555–565. https://doi.org/10.1016/j.coastaleng.2007.01.002

Turner, I. L., Harley, M. D., Short, A. D., Simmons, J. A., Bracs, M. A., Phillips, M. S., & Splinter, K. D. (2016). A multi-decade dataset of monthly beach profile surveys and inshore wave forcing at Narrabeen, Australia. *Scientific Data*, *3*, 1–13. https://doi.org/10.1038/sdata.2016.24

Vitousek, S., Barnard, P. L., Limber, P., Erikson, L., & Cole, B. (2017). A model integrating longshore and cross-shore processes for predicting long-term shoreline response to climate change. *Journal of Geophysical Research: Earth Surface*, *122*(4), 782–806. https://doi.org/10.1002/2016JF004065

Vos, Kilian, Harley, M. D., Splinter, K. D., Simmons, J. A., & Turner, I. L. (2019). Sub-annual to multi-decadal shoreline variability from publicly available satellite imagery. *Coastal Engineering*, *150*(February), 160–174. https://doi.org/10.1016/j.coastaleng.2019.04.004

Wong, P. P., Losada, I. J., Gatusso, J. P., Hinkel, J., A, K., McInnes, K. L., et al. (2014). Coastal Systems and Low-Lying Areas. In Intergovernmental Panel on Climate Change (Ed.), *Climate Change 2014 – Impacts, Adaptation and Vulnerability: Part A: Global and Sectoral Aspects: Working Group II Contribution to the IPCC Fifth Assessment Report: Volume 1: Global and Sectoral Aspects* (Vol. 1, pp. 361–410). Cambridge: Cambridge University Press. https://doi.org/DOI: 10.1017/CBO9781107415379.010

Wright, L. D., & Short, A. D. (1984). Morphodynamic variability of surf zones and beaches: A synthesis. *Marine Geology*, *56*(1–4), 93–118. https://doi.org/10.1016/0025-3227(84)90008-2

Wright, L. D., Short, A. D., & Green, M. O. (1985). Short-term changes in the morphodynamic states of beaches and surf zones: An empirical predictive model. *Marine Geology*, *62*(3–4), 339–364. https://doi.org/10.1016/0025-3227(85)90123-9

Xiong, M., Liu, P., Cheng, L., Deng, C., Gui, Z., Zhang, X., & Liu, Y. (2019). Identifying time-varying hydrological model parameters to improve simulation efficiency by the ensemble Kalman filter: A joint assimilation of streamflow and actual evapotranspiration. *Journal of Hydrology*, *568*(November 2018), 758–768. https://doi.org/10.1016/j.jhydrol.2018.11.038

Yates, M. L., Guza, R. T., & O'Reilly, W. C. (2009). Equilibrium shoreline response: Observations and modeling. *Journal of Geophysical Research: Oceans*, *114*(9). https://doi.org/10.1029/2009JC005359

578 Young, I. R., & Ribal, A. (2019). Multiplatform evaluation of global trends in wind speed and
579 wave height. *Science*, *552*(May), 548–552. https://doi.org/10.1126/science.aav9527

580